Eur. Phys. J. C 4, 231–247 (1998)
DOI 10.1007/s100529800874

THE EUROPEAN PHYSICAL JOURNAL C
© Springer-Verlag 1998

Systematic study of low-mass electron pair production in p–Be and p–Au collisions at 450 GeV/c

G. Agakichiev[1a], M. Appenheimer[2], R. Averbeck[3], F. Ballester[4], R. Baur[5b], A. Brenschede[2], J. Diaz[4], A. Drees[5], U. Faschingbauer[1], J.L. Ferrero[4], P. Fischer[5], Z. Fraenkel[6], M. Franke[2], Ch. Fuchs[1c], E. Gatti[7], P. Glässel[5], Th. Günzel[5], C. P. de los Heros[6], F. Hess[1], R. Holzmann[3], V. Iourevitch[8a], D. Irmscher[5], C. Jacob[1], W. Kühn[2], B. Lenkeit[5], H. Löhner[9], A. Marin[4], F.M. Marques[4], G. Martinez[4], V. Metag[2], M. Notheisen[2], R. Novotny[2], L. H. Olsen[5], R. Ostendorf[10], Y. Panebrattsev[1a], A. Pfeiffer[5], I. Ravinovich[6], P. Rehak[11], M. Sampietro[7], A. Schön[5], J. Schukraft[8], Y. Schutz[10], S. Shimansky[8a], A. Shor[6], R.S. Simon[3], H. J. Specht[5], V. Steiner[6], S. Tapprogge[5], G. Tel-Zur[6d], I. Tserruya[6], Th. Ullrich[5], H. Wilschut[9], J. P. Wurm[1]

[1] Max-Planck-Institut für Kernphysik, D-69117 Heidelberg, Germany
[2] II. Physikalisches Institut der Universität Gießen, D-35392 Gießen, Germany
[3] GSI, D-64220 Darmstadt, Germany
[4] Instituto Fisica Corpuscular, E-46100 Burjassot Valencia, Spain
[5] Physikalisches Institut der Universität Heidelberg, D-69120 Heidelberg, Germany
[6] Weizmann Institute of Science, Rehovot 76100, Israel
[7] Politecnico di Milano, I-20133 Milano, Italy
[8] CERN, CH-1211 Geneva 23, Switzerland
[9] Kernphysisch Versneller Institut, NL-9747AA Groningen, Netherlands
[10] GANIL, F-14021 Caen, France
[11] Brookhaven National Laboratory, Upton, NY 11973, USA

Received: 2 July 1997 / Published online: 5 June 1998

Abstract. In a joint effort the CERES/NA45 and TAPS collaborations have measured low-mass electron pairs in p–Be and p–Au collisions at 450 GeV/c at the CERN SPS. In the range covered up to ≈ 1.5 GeV/c^2 the mass spectra from p–Be and p–Au collisions are well explained by electron pairs from decays of neutral mesons. For p–Au our result is new. For p–Be, the simultaneously measured electron pairs and photons served as a direct measure of the η Dalitz decay contribution to the inclusive pair spectrum in which instrumental uncertainties are highly reduced. We confirm the earlier finding of HELIOS-1 with significantly reduced systematic uncertainties of 23% in the mass range below 450 MeV/c^2, and of 28% in the mass range above 750 MeV/c^2 at 90% confidence limit. Any unconventional source of electron pairs is limited by these error margins as the percentage fraction of the hadronic contribution.

1 Introduction

The investigation of low-mass lepton pair production ($m_{pair} < 1$ GeV/c^2) in hadronic collisions extends back over more than two decades [1]. For a long time most of the experiments observed a lepton pair yield above the contribution expected from hadronic sources. A number of theoretical models had been proposed to explain these anomalous pairs, e.g. hadronic Bremsstrahlung [2], the soft-annihilation-model from Bjorken and Weisberg [3] and the model of the quark-gluon-plasma by Shuryak [4].

More recently, the HELIOS-1 collaboration observed that the yield of e^+e^- and $\mu^+\mu^-$ pairs in p–Be collisions at 450 GeV/c can be accounted for by decays of neutral mesons produced in the reaction [5]. The upper limits of any unconventional source of electron pairs were given as 37-48% of the hadronic decays, depending on mass, in the range $0.2 < m < 0.46$ GeV/c^2. The simultaneous measurement of lepton pairs and photons allowed to directly measure certain Dalitz decay modes and thereby significantly reduce systematic errors. It could also be shown, that an apparent enhancement deduced from earlier experiments was due to an underestimation of the relevant hadron production cross sections, in particular the cross section for the η meson.

In order to increase the sensitivity to possible deviations from conventional sources like those proposed in [2–4], further investigations of hadronic cross sections and

[a] visiting from JINR, Dubna, Russia
[b] Doctoral Thesis of R. Baur, University of Heidelberg (1994)
[c] Doctoral Thesis of Ch. Fuchs, University of Heidelberg (1996)
[d] Ph.D. Thesis of G. Tel-Zur, Weizmann Institute of Science (1996)

of the decay modes into lepton pairs are necessary. Precise dilepton data from p–p and p–A collisions are also needed as reference data in searching for new physics phenomena in heavy ion collisions. An analysis of the inclusive p–Be data [6] to be presented here was in fact providing the necessary scale of conventional sources for detecting an enhancement of low-mass electron pairs in S–Au collisions beyond the expectation from hadron decays [7].

The CERES/NA45 collaboration together with the TAPS collaboration performed a coincident measurement of electron pairs and photons in 450 GeV/c p–Be and p–Au collisions at the CERN SPS. The goal was to provide more accurate data on neutral meson production at mid rapidity and to reduce the uncertainties in the determination of hadronic contributions to the dilepton spectrum considerably [8]. The Dalitz decays of neutral mesons (π^0,η) have been fully reconstructed via their $e^+e^-\gamma$ decay branch, detecting the e^+e^- pair by the Cherenkov spectrometer and the photons in the electromagnetic calorimeter of TAPS [6,9,10]. Precise data for the π^0, η and ω mesons were obtained from their $\gamma\gamma$ and $\pi^0\gamma$ decay branches, respectively, which are presented in an accompanying paper [11].

2 Experimental setup and data taking

2.1 Apparatus

The CERES spectrometer [12] was installed in 1990 at the H8 beam line of the CERN SPS North Area and started operation in 1991. After data taking in spring 1992 with sulphur and proton beam the experimental setup was supplemented with the BaF_2 calorimeter [13] of the TAPS collaboration in 1993 for a simultaneous precision measurement of neutral meson production in proton induced collisions. An overview of the 1993 setup is shown in Fig. 1. A detailed description of the individual setups can be found in [11,12]. Here we summarize the most relevant features of the combined detector system.

CERES is an experiment dedicated to the measurement of electron pairs in the low-mass range of 0.2 GeV/c^2 $\leq$m$\leq$1.5 GeV/c^2, at ultra-relativistic energies. The spectrometer was designed to measure an extremely weak source at a level of about 10^{-5} pairs per π° for m$\geq$ 0.2GeV/c^2, which is the expectation of electron pairs originating from electromagnetic decay of mesons produced. In many ways the response of the spectrometer to hadronic species has been minimized.

Two ring-imaging Cherenkov counters (henceforth referred to as RICH-1,2) are combined with a magnetic field of azimuthal symmetry to identify and track electron pairs. Due to the high Cherenkov threshold ($\gamma_{th} \approx 32$), it is a very small fraction of all charged hadrons that produces Cherenkov photons in the gas radiators: only about 2% of the pions have momenta above the threshold of 4.5 GeV/c, and most of them can be identified by their ring radius.

The azimuthal deflection for momentum determination is provided by a super-conducting double solenoid between the two detectors which leaves the polar angle θ nearly unchanged. The magnetic field (sketched in Fig. 1) is compensated to nearly zero in the region of the first RICH radiator thus preserving the original direction of the particles. This fact enables identification of close pairs from conversions and Dalitz decays. A set of correction coils shape the field in the second RICH radiator such that it points back to the target, ensuring straight trajectories and therefore sharp ring images.

The Cherenkov photons from the RICH radiators are registered in two UV detectors, which are placed upstream of the target and are therefore not subject to the large flux of forward going charged particles. The information of the detectors is read out via two-dimensional arrays of about 50,000 pads each. Photon hit amplitudes are exponentially distributed and the gain of the UV-detectors is kept in the range 2–4·10^5. The signal of a single-electron avalanche is typically distributed over 5–10 pads. The signal-to-noise level for the central pad of a photon hit is 30 or larger, resulting in a high ($\geq$90%) detection efficiency for a single electron avalanche.

The spectrometer covers the pseudo-rapidity region $2.1 < \eta < 2.65$ near mid-rapidity with 2π azimuthal coverage and a broad range of transverse momenta including $p_\perp = 0$. At very low masses, the acceptance is effectively limited by kinematic cuts in the off-line analysis (see Sect. 3.4). At 200 MeV/c^2, the pair acceptance is about equal to the geometrical acceptance of the virtual photons; it drops by roughly a factor of ten above masses of several hundred MeV/c^2.

The amount of material in the acceptance downstream of the target was kept at $\simeq$1.3% of a radiation length in order to minimize conversions of photons and multiple scattering. The largest share (0.41%) is still from the mirror of RICH-1. Yet, this is a construction custom-made for low $X/X_\circ$ of a 1.1 mm thick spherical shell of polyester laminate on a carbon fiber matrix exhibiting optical quality[1].

Background from photon conversions is also reduced by employing special target geometries. The beryllium target is shaped as a wire 1.2 mm in diameter and 30 mm long which results in 7.4% of an interaction length, but only 0.8% of a radiation length within the CERES acceptance. For the same reason, the gold target is segmented into 29 Au disks, 600 μm in diameter of 50 μm thickness each, which are lined up along the beam axis with 2.9 mm spacing (2.3% interaction length, 1.1% effective radiation length).

A silicon pad detector [14] segmented into 64 pads supplies information about charged particle multiplicity for both first-level triggering (FLT) and off-line analysis[2].

The BaF_2 calorimeter of the TAPS group was positioned 6 m downstream from the target. A total of 378 BaF_2 detectors, with 12 radiation lengths, were arranged in a hexagon around the beam axis covering a pseudo-rapidity range $3.0 < \eta < 4.0$ which is adjacent to that of CERES, $2.1 < \eta < 2.65$ without overlap. This keeps

[1] supplied by Mannesmann Technology

[2] A second silicon detector, a 3-inch diameter silicon drift detector, was installed but not used in the analysis

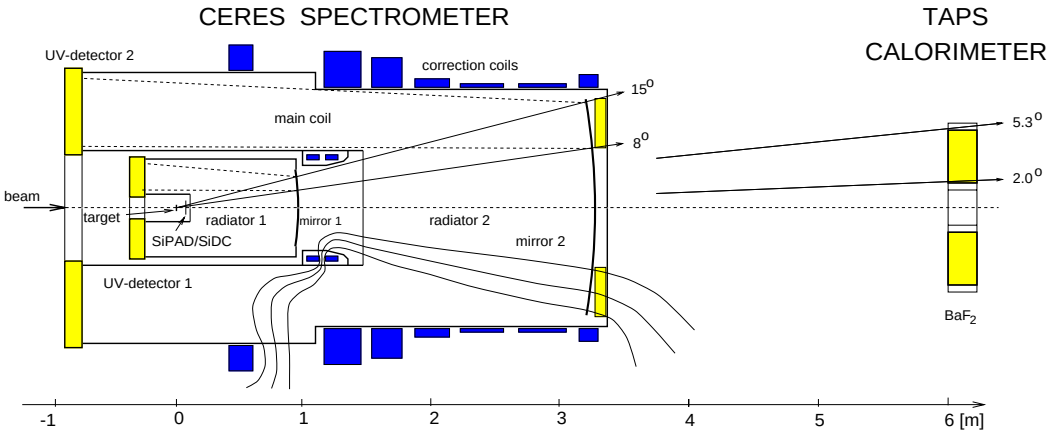

Fig. 1. The combined CERES/TAPS spectrometer for the 1993 measurement at the 450 GeV proton beam of the CERN SPS

reasonable acceptance and avoids significant amounts of material, like the second RICH mirror, in front of the calorimeter. Moreover, this placement avoids systematic errors possibly arising from overlap of electron and photon showers.

2.2 Trigger

Since the production rate of genuine e^+e^- pairs in hadron collisions – those which do not originate from photon conversions – is so small, the need of an effective event selection is obvious. CERES uses a three-stage trigger system. The first-level trigger FLT is based on charge multiplicity information deduced from the silicon pad detector. It ensures target interactions by requiring a certain minimum number of hit pads in coincidence with an incoming beam particle. In the higher trigger levels the event is searched for e^+e^- pairs. Pairs of interest, i.e. with invariant masses above 200 MeV/c^2, have large opening angles and lead to two isolated rings. In contrast, the abundant background from conversions and π^0 Dalitz decays has small opening angles resulting in overlapping ring images. Thus the higher level triggers identify events with two distant ring candidates. Both triggers are based on parallel processing of the data from the first RICH detector. A complete description of the trigger electronics may be found in [12, 15].

The first higher level trigger (intermediate-level trigger ILT) exploits the low multiplicity of proton-induced reactions. In proton-induced interactions the UV-detectors are virtually empty for most events, therefore already a rough ring recognition allows to significantly reduce the number of recorded events. Technically, 8×8 pads are combined to one channel resulting in a grid of 35×35 channels for the full detector. Subsequently a threshold is applied to all channels and the grid is searched for two distinct groups of channels. Within 35 μs 90% of the events are rejected while $\sim$ 90% of all events with e^+e^- pairs are kept.

The last level, for historical reasons called second-level trigger SLT, operates on a more granular information containing every second vertical and horizontal pad of the first UV detector. A systolic array of 160×160 processors allows a fully parallel analysis of the image. It performs a point–to–ring Hough transformation which is equivalent to counting hit pads in a circular mask for each possible ring center. To make the algorithm robust against background hits the mask has a positive correlation region at the asymptotic Cherenkov ring diameter and a negative portion inside and outside of this diameter. A similar algorithm, described in Sect. 3.1, is used in the off-line analysis. Ring candidates are identified by a minimum number of hits found within the mask. In a second correlation step all ring candidates that are closer than 30 mrad to each other are rejected. Finally, within 140 μs after the collision events with two separated ring candidates are selected. Note that the trigger scheme introduces a bias against pairs of small opening angles. This effect will be discussed in Sect. 2.3.

2.3 Data taking and trigger performance

Data were taken with beryllium (Be) as a proton- or neutron-like target and gold (Au) as heavy target. During 4 months of running with the e^+e^- pair trigger a total of $10.3 \cdot 10^6$ and $2.6 \cdot 10^6$ events were accumulated for p–Be and p–Au, respectively, that qualified for the full analysis chain. The trigger dramatically enriches the amount of events containing e^+e^- pairs in the recorded data sample. The enrichment factor $F_T = R_T \cdot b_{FLT} \cdot \epsilon_T$ is the product of three factors, the event reduction R_T, i.e. the ability to reject undesired events, the efficiency ϵ_T to recognize e^+e^- pairs, and the so-called FLT bias b_{FLT}.

The multiplicity thresholds in the first level trigger were set to $N_{ch} \geq 4$ for p–Be and $N_{ch} \geq 6$ for p–Au in $2 < \eta < 3$. For events with an e^+e^- pair in the acceptance, the effective multiplicity threshold is reduced by ~ 2. Therefore, the first level trigger covers a larger fraction of the inelastic cross section for events with an e^+e^- pair than without it. The FLT bias b_{FLT} is given by the ratio of interactions with $N_{ch} \geq 2$ ($N_{ch} \geq 4$) to $N_{ch} \geq 4$ ($N_{ch} \geq 6$). The ratio was monitored continuously (see Fig. 2), yielding an average value of 2.4 in p–Be and 1.4 in p–Au.

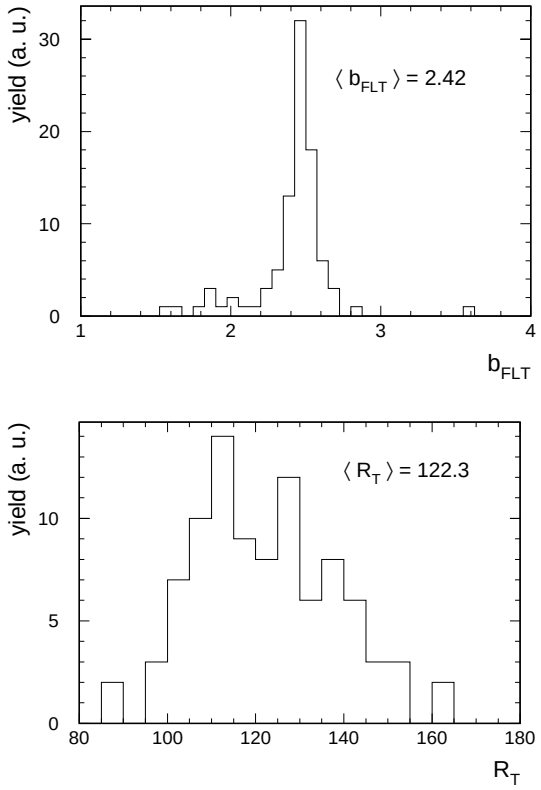

Fig. 2. The FLT bias b_{FLT} (top) and the rejection factor R_T of the combined ILT+SLT (bottom) in p–Be

The event reduction due to the ILT as well as the combined ILT+SLT reduction were monitored on-line. As shown in Fig. 2, the combined reduction yields an average value R_T of 122 for p–Be. For p–Au we find $R_T = 106$. The efficiency ϵ_T of the combined ILT+SLT is ~ 0.60, both in p–Be and p–Au. This value is obtained using a trigger emulator software that is fed with Monte-Carlo events. A more detailed discussion of this efficiency is given in Sect. 3.4.

The trigger enriches the pair samples by a factor F_T of 175 for p–Be and of 90 for p–Au. Thus the analyzed data samples quoted above correspond to $1.8 \cdot 10^9$ and $2.3 \cdot 10^8$ minimum bias events for p–Be and p–Au, respectively.

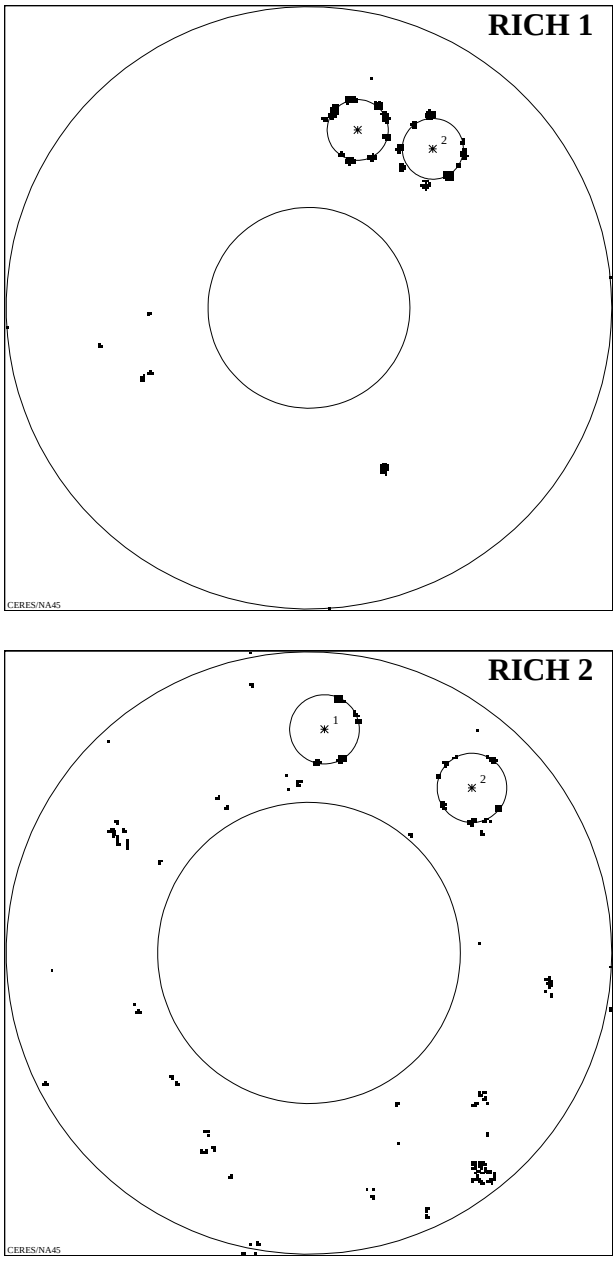

Fig. 3. An event with an e^+e^- pair in RICH-1 and RICH-2. The structure of Cherenkov rings consisting of individual photon hits is clearly visible. The event is nearly free of background

3 Reconstruction of e^+e^- pairs

3.1 Electron recognition

The reconstruction of electron rings is based solely on the information of the two RICH detectors. An example of a raw p–Be event is displayed in Fig. 3. The structure of photon hits that is associated with Cherenkov rings is clearly visible, while the rest of the event is nearly free of background. Rings are reconstructed without an a priori knowledge of the ring centers. The event is first cleaned from background signals originating from electronic noise and physics sources like highly ionizing particles, which complicate the ring recognition. Subsequently, the event is searched for ring candidates. For each pad with an amplitude above some threshold, a point–to–ring Hough transformation is performed with a ring mask of diameter equal to that of an asymptotic electron ring. In the transformed image a peak appears at the location of the center of an electron ring (see Fig. 4). In the vicinity of these candidates, single photon hits are reconstructed, and a ring of asymptotic radius is fitted to these hits. Finally, various ring quality criteria are applied to distinguish genuine Cherenkov rings from fake rings originating from random combinations of hits.

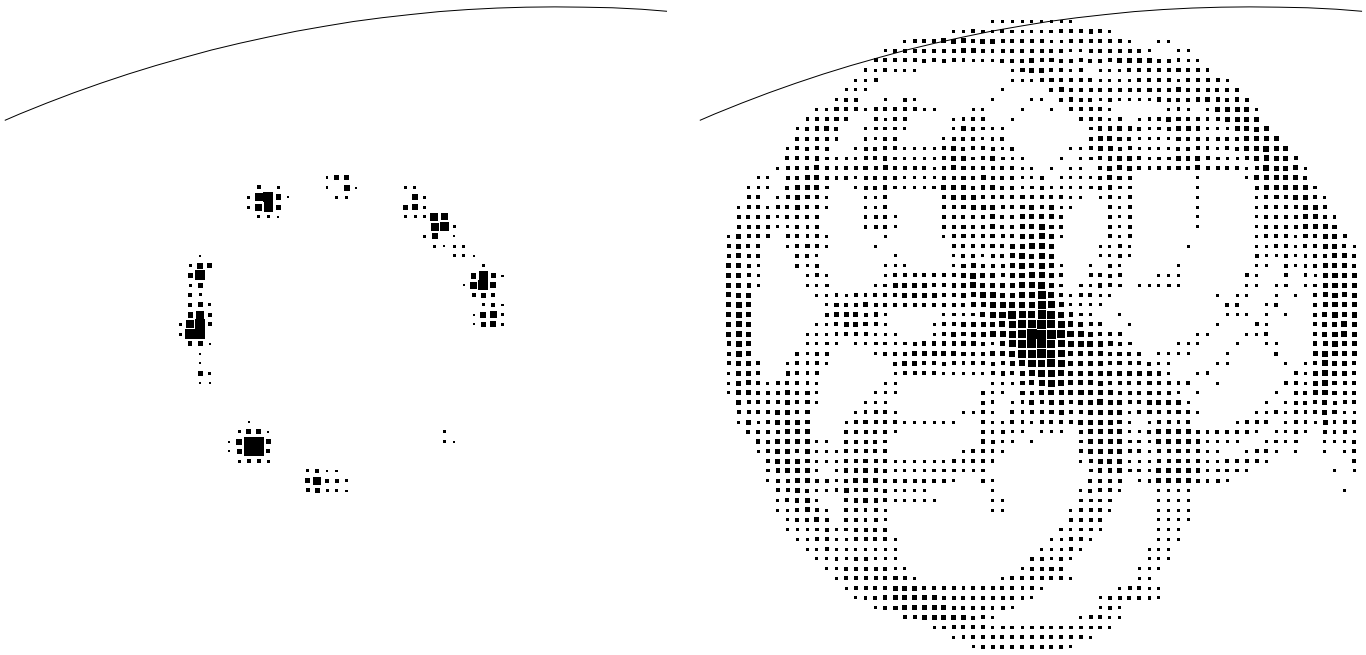

Fig. 4. Photon hits, registered by the electronic charge induced on the pad plane of the UV detector, form a Cherenkov ring of radius R (left). The Hough image of each photon hit is a circular band with Hough radius R_H of the mask, displayed in the correlation plane (right). For $R_H = R$, the images ideally would have one point in common, the center of the Cherenkov ring

3.2 Track and pair reconstruction

The accepted rings in both RICH detectors are combined to tracks, identified by their common angle θ to the beam axis. The magnetic field deflects particles in azimuth inversely proportional to their momenta, i.e. $\Delta\phi = 120\text{mrad}/p$, p in GeV/c. In order to minimize ambiguities in the track assignment, we limit the deflection $\Delta\phi$ between the RICH detectors by accepting tracks with $p_\perp > 50$ MeV/c only. Particles deflected azimuthally suffer a small θ deflection towards the beam axis, i.e. $\Delta\theta = 0.0556(\Delta\phi)^2$ /rad. Figure 5 displays the correlation between $\Delta\theta$ and $\Delta\phi$ for electron and positron tracks. The width of the distribution along $\Delta\theta$ limits the match quality and reflects the finite resolution which deteriorates with decreasing momentum due to multiple scattering of the particles between the RICH detectors.

The momentum resolution of the spectrometer is given by the track resolution, which itself is determined by the ring center resolution and deteriorated by multiple scattering. In the high-momentum limit, i.e. neglecting multiple scattering, the track resolution is $\sigma_\theta = 1.22$ mrad [12]. This corresponds to the width of the $\Delta\theta$ distribution in Fig. 5 for $\Delta\phi \sim 0$. The resulting momentum resolution is $\sigma_p/p = 5.3\%p$, p in GeV/c, at $\theta = 11°$.

In Fig. 6 typical track patterns are sketched. Most tracks originate from $\gamma \to e^+e^-$ and $\pi^0 \to e^+e^-\gamma$, i.e. pairs of from small mass and small opening angle. Since there is no field in the first RICH, the opening-angle information is preserved and allows to recognize close pairs of conversions and Dalitz decays. Their rejection is vital

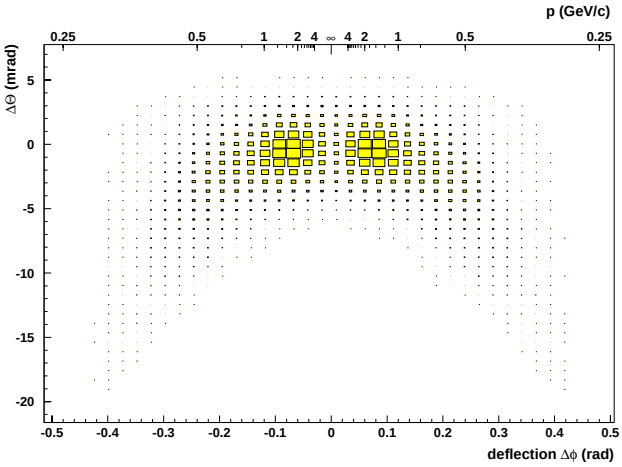

Fig. 5. Density profile of electron and positron tracks in the $\Delta\phi$, $\Delta\theta$ plane. $\Delta\phi$ is the primary deflection in azimuth proportional to $1/p$; see the momentum scale on top. Note that $\Delta\theta$ is measured in mrad, but $\Delta\phi$ in radians

for reduction of the combinatorial pair background (see below).

Pairs are reconstructed according to the opening angle in three steps. In the first step only pairs with an opening angle smaller than the double ring resolution of ~ 10 mrad, i.e. sharing the same ring in RICH-1 (V-tracks), are reconstructed and removed from the sample. In the second step close pairs with an opening angle lower than 65 mrad are reconstructed. They mostly originate from π^0 Dalitz decays. The tracks of these pairs are not taken into

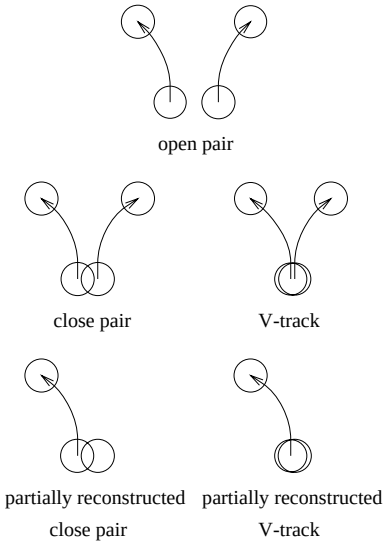

Fig. 6. All possible types of track patterns that may occur in the events. The signal of genuine pairs, with invariant mass $m > 200$ MeV/c^2 consists of open pairs. Close pairs mostly originate from π^0 Dalitz decays and V-tracks mostly from γ conversions. Partially reconstructed pairs look like single track candidates and are the major source of combinatorial pair background

account for further pair combinations. All other tracks are combined to open pairs.

3.3 Background rejection

At this stage of the analysis, most pairs are still combined of tracks from photon conversions and π^0 Dalitz decays which escaped full reconstruction due to a limited detector acceptance and the inefficiency in reconstruction. This combinatorial pair background is about 10–20 times larger than the pair signal itself. Clearly, the central problem of the analysis is to reject as many of the background pairs as possible without vetoing the signal. Optimization has to be done therefore in a way to balance background rejection power, discussed here, and signal efficiency, discussed in Sect. 3.5. A convenient measure of statistical significance is the effective number of signal pairs S_{eff} that corresponds to a hypothetical background-free measurement of identical statistical error, $S_{eff} = S/(1 + 2B/S)$.

Conversions and π^0 Dalitz decays need to be identified even if the pair is not fully reconstructed. Again, the necessary rejection power is provided by the small opening angle of these pairs. For conversions the average opening angle is ∼5 mrad, thus most of the conversions give rise to unresolved double rings. Only 10–20% of these conversions are fully reconstructed as V-tracks. Partially reconstructed V-tracks (see Fig. 6), i.e. those with one missing ring in RICH-2, result in apparent single tracks. A significant fraction of these can be removed by analyzing the number of Cherenkov photons associated to the ring in the first RICH. Many photon hits on double rings overlap, therefore we do not count the hits, but rather analyze the analog sum of all signals in a ring mask. Cutting at 1.6 times the average amplitude of a single ring, 80% of the γ conversions are rejected at an efficiency of 85% for single tracks.

Not fully reconstructed background pairs with opening angles just above the double ring resolution, i.e. mostly π^0 Dalitz decays, can be identified if the second ring in RICH-1 was reconstructed. We therefore remove all tracks from the sample which have a second ring in RICH-1 closer than 45 mrad to the inspected track if that ring is not part of another track. This topology corresponds to the type termed partially reconstructed close pair in Fig. 6. The efficiency of this cut is 90% and it removes one half of the background pairs still present.

Some high-momentum pions are misidentified as electrons. In order to reject such tracks we require that the ring diameter is within 5% equal to the asymptotic diameter. In addition, we reject tracks with a momentum above 7 GeV/c.

Table 1. Evolution of the electron pair signal S, signal-to background ratio S/B and the effective signal S_{eff} with various analysis cuts (see text) proceeding from top to bottom, for p–Be and p–Au. Input data are pairs with $m_{e^+e^-} > 200$ MeV/c^2, $p_\perp > 50$ MeV/c and opening angle $\theta_{ee} > 35$ mrad

	p–Be			p–Au		
	S	S/B	S_{eff}	S	S/B	S_{eff}
Input data	7975	1/10.1	376	1741	1/16.6	51
Pion rejec.	6614	1/5.8	525	1428	1/9.0	75
Close ring	6000	1/3.3	790	1297	1/5.3	112
Ring ampl.	5068	1/2.0	1014	1068	1/3.6	130

3.4 Results

The number of electron pairs in p–Be and p–Au with $m_{e^+e^-} > 200$ MeV/c^2, the signal-to-background ratio S/B and the background free equivalent S_{eff} are listed in Table 1 cumulatively after each rejection cut. The combined effect of all cuts results in an improvement of the S/B ratio by a factor of ∼ 5, both for the p–Be and the p–Au sample. In order to avoid the trigger bias on pairs with small opening angles only pairs with opening angles $\theta_{ee} >$ 35 mrad are taken into account.

The remaining combinatorial background in the e^+e^- sample is determined by counting the like-sign pairs. The pair signal S is extracted by subtracting the like-sign contribution from the e^+e^- sample as $S = N_{+-} - R(N_{++} + N_{--})$. The R factor would be bigger than 1 if the probability to collect a background electron pair would be higher for pairs of oppositely charged tracks than for like-sign pairs. This could be due to correlations at the level of particle production or to correlations introduced by the detector's acceptance or by the trigger. In our experiment, most background pairs result from associating two tracks belonging to two different decay processes, mostly conversions ($\gamma \to e^+e^-$) and π° Dalitz decays ($\pi^0 \to e^+e^-\gamma$),

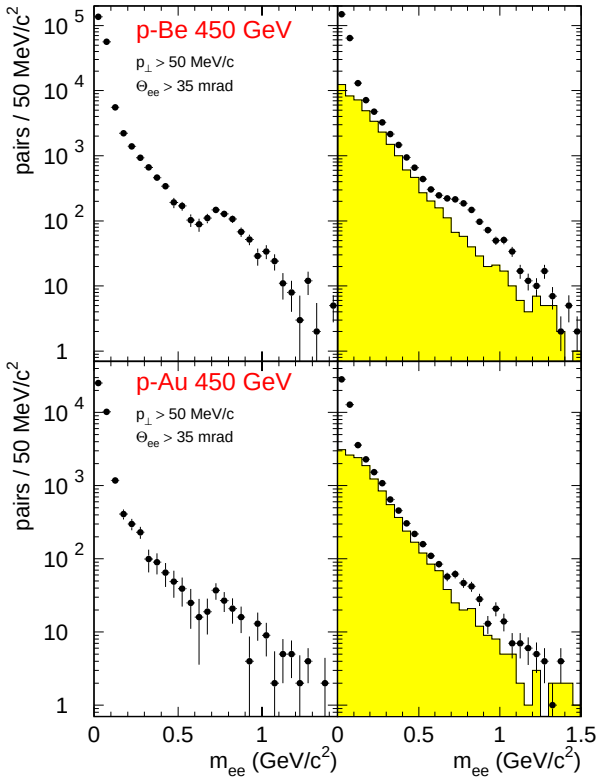

Fig. 7. Invariant mass distribution of the signal pairs after subtraction of combinatorial background on left side. Spectra of unlike-sign pairs (*data points*) before subtraction of the like-sign pairs (*histogram*) on right side. Top row: p–Be, bottom row: p–Au

simultaneously occurring in the same collision. Since this source of background pairs is of a purely combinatorial nature and since there is no bias introduced by the trigger or by the acceptance, all charge combinations are equivalent. Thus, in our case R is equal to 1.

The final p–Be (p–Au) sample for $m_{e^+e^-} > 200$ MeV/c^2 consists of 5068 (1068) pairs with a S/B ratio of 1/2.0 (1/3.6). Figure 7 shows the invariant mass distribution of like- and unlike-sign pairs as well as the subtracted spectra for p–Be and p–Au, respectively. As expected from the π^0 and η Dalitz decays, the subtracted distributions strongly decrease with mass. The structure from the direct decays $\rho/\omega \to e^+e^-$ at ~ 780 MeV/c^2 is clearly visible. The measured width of the ρ/ω peak gives a mass resolution of $\sigma_m/m \sim 11\%$. Although this agrees with the expected value from the measured momentum resolution of the CERES spectrometer, it is considerably worse than the $\sigma_m/m \sim 7\%$ at m_ω we would expect on the basis of the measured single-hit resolutions in the RICH detectors. We have no explanation for this long-standing problem of an inconsistency between single-hit and ring-center resolution in RICH-1. This problem is overcome with the precise external tracking added for the continuation of the experiment with the lead beam [16].

3.5 Reconstruction efficiency

The pair reconstruction efficiency is a measure of the ability to recognize electron pairs within the spectrometer acceptance. It depends on the trigger efficiency and the off-line reconstruction efficiency including all rejection cuts that are applied in order to reduce the combinatorial background. The trigger and pair reconstruction efficiencies are determined using an event generator (see Sect. 6) which generates electron pairs in the spectrometer acceptance, each of the two electrons with $p_\perp > 50$ MeV/c, together with a complete Monte-Carlo simulation of the detector response, in particular of the RICH detectors. The simulation of the detector response is based on measured quantities like the number of Cherenkov photons per ring, hit amplitude, hit size, position resolution and the magnetic field deflection.

The Monte-Carlo generated rings are overlayed on untriggered data for realistic background conditions. The combined events are passed through the off-line analysis chain, including the full trigger emulation. The pair efficiency is defined as the ratio between the number of reconstructed to the number of generated Monte-Carlo pairs.

Figure 8 shows the trigger and off-line pair reconstruction efficiency (here without applying any rejection cuts) as a function of the pair opening angle θ_{ee}. Towards small opening angles, i.e. < 40 mrad, the trigger efficiency decreases dramatically due to finite double ring resolution of the SLT algorithm. Around 60 mrad, which is the Cherenkov ring diameter, the trigger efficiency exhibits a characteristic structure: a maximum with a shallow minimum at smaller and larger opening angles. This structure is also an effect of the SLT algorithm. For opening angles equal to the ring diameter, hits in the region of overlapping rings populate the positive part of both circular masks around the potential ring centers, and thereby increase the trigger efficiency for the pair. In contrast, for opening angles just above or below the ring diameter, hits from the partner ring fall into the negative region of the mask which reduces the efficiency of the trigger. At opening angles $\theta_{ee} > 80$ mrad, the trigger efficiency saturates at about 60%. The off-line reconstruction efficiency of pairs which pass the trigger is further reduced by requiring two rings in RICH-2. This efficiency is $\sim 68\%$ and together with the trigger efficiency of 60% we arrive at a total pair reconstruction efficiency of 40% for opening angles $\theta_{ee} > 80$ mrad.

Figure 8 also shows the ratio of the measured opening angle distribution to the expected distribution for hadron decays. It is normalized to 40% for opening angles $\theta_{ee} > 80$ mrad. The excellent agreement with the opening-angle dependence of the pair reconstruction efficiency determined from the Monte-Carlo simulation demonstrates the consistency in our present understanding of the trigger.

The pair reconstruction efficiency before and after the rejection cuts is shown in Fig. 9 as a function of the invariant pair mass. At low masses the opening angles are small and therefore the efficiency decreases according to Fig. 8. The rejection cuts introduce a further opening-angle dependence and therefore mass-dependent efficiency. This is

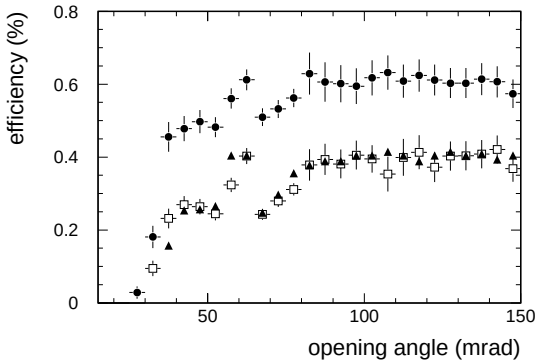

Fig. 8. Trigger and pair reconstruction efficiency as a function of opening angle between electron and positron; no rejection cuts are applied. The reconstruction efficiency derived from data (*full triangles*) agrees well with that derived from Monte-Carlo simulations (*open squares*). On top, the Monte-Carlo generated trigger efficiency (*full circles*)

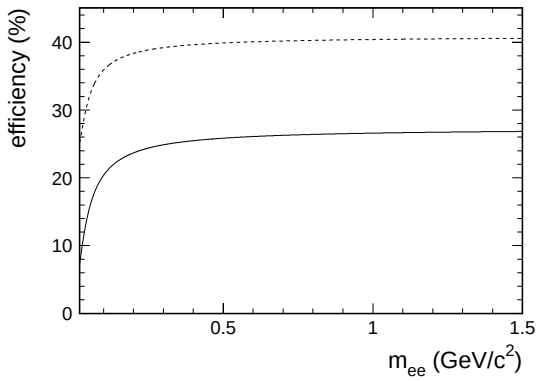

Fig. 9. Reconstruction efficiency of electron pairs as a function of the invariant pair mass. The *dashed line* shows the efficiency before, the *solid line* after the rejection cuts. The drop in efficiency towards very low masses originates from its opening-angle dependence

dominantly caused by the sum-amplitude cut, since pairs with small opening angles have partially overlapping rings in RICH-1. The efficiency of the rejection cuts is $\sim 65\%$ for $m_{ee} > 200$ MeV/c^2. The overall pair reconstruction efficiency is $\sim 25\%$ for $m_{ee} > 200$ MeV/c^2.

4 Photon reconstruction

A detailed description of the photon reconstruction and the detector calibration can be found in the accompanying paper [11]. Here we give a brief summary only. Photons are measured by reconstructing showers in the BaF_2 calorimeter. Since the calorimeter operates without vetoing charged particles, photon identification has to be realized in the off-line shower analysis. Signals from minimum-ionizing particles are removed by requiring a minimum shower energy of 300 MeV or higher. We exploit the fact that the lateral width of electromagnetic showers is considerably smaller than that of hadronic ones, and apply a so-called dispersion cut on the second central moment of the lateral distribution. Special emphasis is given to the energy calibration of the detector. It needs to be mentioned that the final iterative calibration of temperature-dependent gain variations using the accepted π° mass could only be realized with the data presented in [11]. In this analysis the number of events recorded over a few hours, a typical time scale for gain variations, was too small to reconstruct the $\pi^\circ \to \gamma\gamma$ decay. The energy resolution is therefore deteriorated by $\sim 40\%$ and reaches only 5 and 7% at 170 MeV and 10 GeV.

5 Reconstruction of Dalitz decays

The coincident measurement of e^+e^- pairs in the spectrometer and photons in the calorimeter allows for the kinematically complete reconstruction of the π^0, $\eta \to e^+e^-\gamma$ Dalitz decays. In principle, the contribution of each type of Dalitz decay to the inclusive electron pair mass spectrum is directly determined from the exclusive measurement by projecting the 3-body phase space onto the 2-body m_{ee} axis. In practice, the situation is more complicated. Due to the limited acceptance and reconstruction efficiency of the photon, only a small fraction of the Dalitz decays will be reconstructed while it has to compete with a large combinatorial background. But the method still retains its principal advantage to quantitatively account for the Dalitz continua in the mass spectrum without requiring knowledge of all meson production cross sections, the trigger and reconstruction efficiencies.

5.1 $e^+e^-\gamma$ combinations

The $e^+e^-\gamma$ data and the measured combinatorial background are shown in Fig. 10, for π^0 with a threshold of $E_\gamma > 300$ MeV (top), and for the η region (bottom) using a higher threshold of $E_\gamma > 2$ GeV in order to reduce combinatorial background. The electron and positron have $p_\perp > 50$ MeV/c and the opening angle of the pair is $\theta_{ee} > 35$ mrad. The spectra are dominated by the combinatorial background. The π^0 peak is clearly visible, while the signal of the η is hardly recognizable. The background mostly originates from combinations of e^+e^- pairs with the large number of photons from $\pi^0 \to \gamma\gamma$ decays, on average about 5.5 photons with $E_\gamma > 300$ MeV and still about 4 photons with $E_\gamma > 2$ GeV per event in the calorimeter acceptance. In contrast, only for every $\sim$5th reconstructed e^+e^- pair from a Dalitz decay the photon will fall in the calorimeter acceptance. This seems to indicate that combinatorial background could be reduced by rejecting those photon pairs that combine to the π^0 mass. However, since the combinatorial background dominates the π^0 mass region in the $\gamma\gamma$ analysis (compare Fig. 3 in [11]) such strategy leads to an unacceptable efficiency loss in the signal.

5.2 Background subtraction

In order to extract the number of π^0 and η mesons an accurate measurement of the background is essential. One

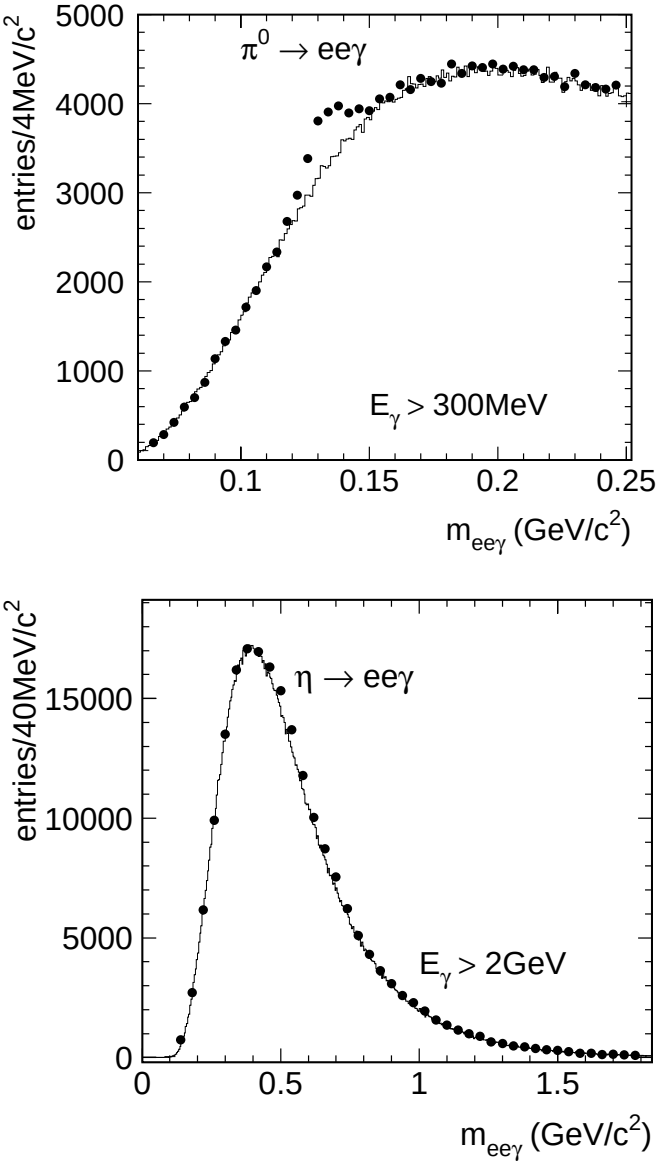

Fig. 10. Invariant mass spectrum of $e^+e^-\gamma$ events in the range of the π^0 with threshold $E_\gamma > 300$ MeV (top), and in the range of the η with threshold $E_\gamma > 2$ GeV (bottom). The *black points* are data, the *solid line* is the measured combinatorial background

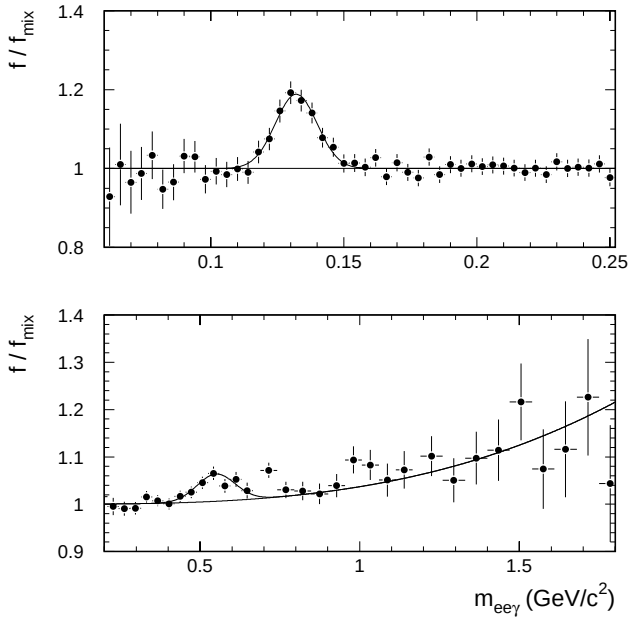

Fig. 11. Ratio $f(m)/f_{mix}(m)$ of the measured $e^+e^-\gamma$ mass spectrum to that obtained by event mixing. The upper panel displays the π^0 region. As the ratio is 1 over the entire range, event mixing requires no further correction. The lower panel shows the η region. Here, event mixing deviates progressively at m above the η peak, and the mass dependence of the ratio was fitted with a 3^{rd} order polynomial $P_3(m)$. The Gaussian accounts for the η signal

possibility to obtain the background is the combination of e^+e^- pairs from one event with photons from another event. This event-mixing method describes the combinatorial part of the background, but not necessarily the true background if correlations are present in the events. Also differences in the phase space of electrons and photons between mixed events and true events can lead to discrepancies [17]. A completely different approach to determine the background is the fitting method. The measured invariant mass spectra are fitted with the sum of two functions, one for the description of the background, the other for the description of the signal. This method requires a detailed knowledge of the signal and the background distributions and, moreover, there is the risk to artificially maximize the signal while fitting the background.

Here, we use a combination of both approaches and adopt the fitting method only to correct for the non-combinatorial background fraction. First, we estimate the combinatorial background distribution $f_{mix}(m)$ from event mixing. In order to smooth the background measurement, we combine each e^+e^- pair with photons from ten different events. The mixed event background is normalized to the measured invariant $e^+e^-\gamma$ mass distribution in a region where no signal is expected. In the next step we analyze the ratio $f(m)/f_{mix}(m)$ of the measured invariant $e^+e^-\gamma$ mass distribution to the mixed event background. If the background is described perfectly the ratio will be unity in regions without signal. Deviations from unity point towards a non-combinatorial fraction in the background which is not described by event mixing. A fit of the ratio is then used to correct such deviations.

The top part of Fig. 11 shows the ratio $f(m)/f_{mix}(m)$ for the π^0 meson region. It was normalized to unity in the range $m < 100$ MeV/c^2 and $m > 170$ MeV/c^2. We find a good agreement of mixed event and measured background. No further corrections are needed. The systematic error of the background was judged by normalizing the ratio in different mass regions. The peak to peak change of the background level is 1.2%, which results in a 2.6% uncertainty of the pion yield.

The lower part of Fig. 11 presents the same analysis for the η meson. The ratio $f(m)/f_{mix}(m)$ is normalized to

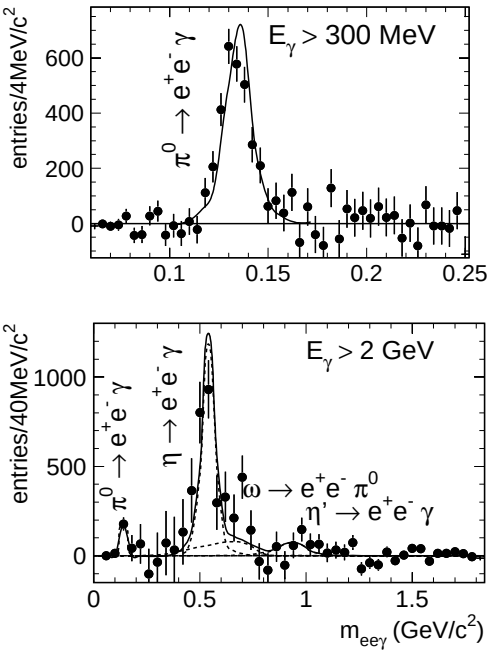

Fig. 12. Invariant mass spectrum of $e^+e^-\gamma$ events after subtraction of the combinatorial background in the range of the π^0 (top) and the η (bottom). Shown are also the generator-simulated line shapes including the η' Dalitz and the incompletely reconstructed ω Dalitz decay

one in the mass range 170 MeV/$c^2 < m <$ 350 MeV/c^2. It increases significantly with mass, which indicates in this case event mixing alone does not reproduce the shape of the background very well. In order to do better, we fit the ratio with a 3^{rd} order polynomial function representing the deviation from the mixed event background, plus a Gaussian at the η mass with a width given by the experimental resolution. The polynomial function $P_3(m)$ is then used to correct the mixed event background. This background is subtracted from the data to extract the η signal, i.e. $S(m) = f(m) - f_{mix}(m) \cdot P_3(m)$. The final η yield is 30% lower than obtained by simply subtracting the background from event mixing. The systematic uncertainty of our procedure was estimated studying fits of the ratio $f(m)/f_{mix}(m)$ with different functions for the background, ignoring or allowing for the contribution of the ω and the η' by separate functions, or excluding the eta mass region from the fit. In these fits the correction changes by less than 2% at the η mass. Due to the poor signal to background ratio this uncertainty translates to a 12.6% systematic error of the η yield.

Figure 12 shows the background-subtracted $e^+e^-\gamma$ spectrum in the range of the π^0 (top) and in the range of the η (bottom). Position and width of the π° and η peaks were determined by a fit of the data (not shown on the figure). The number of reconstructed π^0 and η Dalitz decays was derived by integrating the data in $\pm$ 1.5σ region around the fitted mean. The resulting π^0 and η yields, the S/B ratio and S_{eff} are listed in Table 2. The data was integrated in a $\pm 1.5\sigma$ range in order to maximize the background-free equivalent S_{eff}. Both figures also show

Table 2. Reconstructed Dalitz decays

	S	S/B [%]	S_{eff}
$\pi \to e^+e^-\gamma$	3011±160	13.3	353
$\eta \to e^+e^-\gamma$	2366±230	4.7	106

the expected line shape deduced from the Monte-Carlo simulation. The lower figure includes the simulated η' Dalitz and incompletely reconstructed ω Dalitz decays. Unfortunately, the limited sample of the coincident data does not allow to reconstruct a reliable signal in either case. A small but visible shift of the measured π° peak points towards an imperfection of the calibration.

5.3 Reconstruction efficiency of Dalitz decays

To determine cross sections of the π^0 and η mesons from the number of reconstructed decays listed in Table 2, we must quantify the reconstruction probability of these decays. This requires a knowledge of (a) the reconstruction efficiency of e^+e^- pairs, (b) the photon reconstruction efficiency, and (c) the relative acceptance of the calorimeter. The pair reconstruction efficiency (a) has already been discussed in Sect. 3.4. The photon finding efficiency (b) and the extrapolation from the $e^+e^-\gamma$ kinematic region to the e^+e^- kinematic region are determined by a Monte-Carlo method. First, we generate Dalitz decays. We apply the same cuts imposed by the e^+e^- measurement, i.e. $2.1 < \eta < 2.65$, $p_\perp > 50$ MeV/c, and $\theta_{ee} > 35$ mrad. The relative acceptance for photons is then defined as the fraction of these Dalitz decays with the photon in the calorimeter acceptance of $3 < \eta < 4$.

Photons which enter the calorimeter can be lost due to the energy and the dispersion cut as well as due to pile-up of showers. In order to determine the reconstruction efficiency of photons, showers are simulated in the BaF_2 calorimeter and superposed upon real events. The induced increase in occupancy is negligible. The Monte-Carlo simulation reproduces the observed energy response, the resolution, and the shower profiles in longitudinal and lateral direction. The superposed events are processed through the standard analysis chain including the dispersion and energy cut. All reconstructed photons are then combined with the simulated electron pairs. Like in the data analysis, the number of reconstructed Dalitz decays is determined by integrating the background-subtracted $e^+e^-\gamma$ invariant mass distribution in a $\pm 1.5\sigma$ region around the fitted peak position. Therefore, imperfections of the calibration, like those observed in Fig. 12, or deficiencies in the calorimeter simulation, largely cancel. The photon finding efficiency is determined as the ratio of the number of found to the number of simulated decays. The relative acceptance for $e^+e^-\gamma$ compared to e^+e^-, the photon finding efficiency as well as the resulting total relative efficiency for the exclusive measurement of Dalitz decays, compared to the inclusive measurement of e^+e^- pairs, are listed in Table 3.

Table 3. Relative acceptance for $e^+e^-\gamma$ compared to e^+e^-, the photon finding efficiency, efficiencies for analysis cuts, and the resulting total relative efficiency for the exclusive measurement of Dalitz decays compared to the inclusive measurement of e^+e^- pairs

	π^0	η
Relative acceptance [%]	11	28
Photon finding efficiency [%]	81	90
Dispersion cut [%]	79	84
Energy cut [%]	97	89
Total [%]	6.6	19

Combining the results of Table 3 with the e^+e^- pair reconstruction efficiency, we can estimate the production cross section of the η. Our value is compatible with that measured from the photon decay mode in the same experiment [11], but due to the larger uncertainties it does not improve the latter measurement.

The invariant e^+e^- mass spectrum of the exclusively reconstructed η decays was compared to the measurement of the LEPTON-G collaboration [18]. In order to do so, we have corrected for the m_{ee}-dependent geometrical acceptance of the BaF_2 calorimeter and the pair reconstruction efficiency (shown in Fig. 9). The resulting mass spectrum of the η Dalitz decay agrees well [9] with the generator calculation using the electromagnetic transition form factor derived from the LEPTON-G data; details of the simulation will be given in the following section. We do not show the results here, because the deviation from the Vector Dominance Model as discussed in [19] is in any case very small compared to our errors. Unfortunately, this fact also holds true for the more controversial transition form factor of the ω.

6 Electron-pair yield from neutral meson decays

In order to estimate the contribution of hadron decays to the inclusive e^+e^- pair yield we have developed the GENESIS Monte-Carlo program. In the first step neutral mesons which decay into lepton pairs or photons are generated according to measured production cross sections, $p_\perp$ and y distributions. In the second step they are allowed to decay with known branching ratios simulating the correct decay kinematics. Finally the laboratory momenta of the generated electrons are convoluted with the experimental resolution and acceptance. In order to allow for a meaningful comparison with the data, the simulations are subject to the same filters as the data, namely acceptance, $p_\perp$ and opening angle cut.

The production cross sections of most light mesons were measured in several experiments in p–p or p–A collisions, including our own. In the accompanying paper [11] we have published our results on neutral-meson production at central rapidity and small $p_\perp$ as measured by their $\gamma\gamma$ and $\pi^0\gamma$ decays, together with a compilation of most of the available information. From this data we have derived the input values for the generator calculations; we refer therefore to the acceptance $3.1 \leq y \leq 3.7$ of our own measurement of π°, η and ω which is close to the nucleon–nucleon center of mass rapidity.

The relative meson cross sections normalized to the π^0 yield are given in the first column of Table 4; they were obtained in the following way: the η/π° ratio was taken from our own p–Be measurement [11] as 6.9±0.5%. We have not included NA27 [20] data since the meson/π° ratios reported by NA27 are consistently larger than ours and those of HELIOS-1. The NA27 $p_\perp$ distributions are steeper than suggested by our data, giving rise to higher yield when the cross section is extrapolated to low $p_\perp$.

For ρ and ω, this problem can be circumvented by avoiding the usage of $\rho/\omega/\pi^\circ$ ratios previously determined. Rather, we adopt a weighted 'world average' of 0.36±0.03 for the $\eta/(\rho+\omega)$ ratios of our p–Be and p–Au data, of HELIOS-1 p–Be data, and of NA27 p–p data as listed in Table 1 of [11]. With the accepted η/π° ratio we derive ρ/π°, and ω/π° alike, since both vector mesons are similar in mass and quark content. The relative yield of η' is determined from the upper limit $\eta'/\eta = 0.2$ measured in our experiment [11], which is about 50% lower than the commonly used value of 0.3 extrapolated from high $p_\perp$ data, e.g. [5]. The ϕ/π° ratio was calculated from NA27 data[3].

In order to be able to generate meson total production cross sections, we have extrapolated the numbers to 4π using Gaussian-like rapidity distributions. The width of the π° y-distribution is fixed to 1.8 by data; for all heavier mesons the width is reduced by the ratio $y_{max}(m_i)/y_{max}(m_\pi)$, i.e. the ratio of the kinematic limit ($y_{max} = \ln(\sqrt{s}/m)$) for a particle of mass m_i relative to that for π°. This scaling is in excellent agreement with experimental data (mostly from [20]). The values used in our simulation are given in the third column of the table; the total cross section ratios derived are listed in the second column. Since the widths decrease with mass, the ratios of total cross sections are smaller than for $3.1 \leq y \leq 3.7$. The errors quoted in Table 4 give the systematic uncertainty of our procedure. They result from the statistical and the systematic errors of the available data. For the extrapolation to 4π, they also include some uncertainty in the widths of the y distributions.

The values in Table 4 may be related to the number of charged particles by scaling with π^0/N_{ch}, which is 0.47 ± 0.02 for $y_{cm} = 0$, deduced from NA27 data [20].

In the parameterization used, the cross sections explicitly factorize in $p_\perp$ and y. For the $p_\perp$ distributions

[3] The η/π° and ω/π° ratios determined from NA27 are consistently larger than our values. This could indicate a problem in their π° normalization, then the ϕ/π° ratio would suffer from the same problem. It might have been more appropriate (but was not done) to use the value quoted in Table 4 scaled down by the same factor, which would reduce the ratio ϕ/π° from 0.005 to 0.0033. Since the ϕ meson can almost be ignored in our data due to the small statistics in this mass region, the final result is not affected by our choice for ϕ/π°

Table 4. Relative production cross sections for neutral mesons in the rapidity range $3.1 < y < 3.7$, total cross section ratios and widths s_y (1σ) of the y distributions

	$\frac{(d\sigma/dy)}{(d\sigma_{\pi^0}/dy)}$	$\frac{\sigma_{tot}}{\sigma_{\pi^0,tot}}$	width s_y
$\pi^0(135)$	1	1	1.80
$\eta(547)$	0.069 ± 0.005	0.053 ± 0.004	1.36
$\rho(770)$	0.096 ± 0.010	0.065 ± 0.007	1.24
$\omega(783)$	0.096 ± 0.010	0.065 ± 0.007	1.24
$\eta'(958)$	< 0.014	< 0.009	1.17
$\phi(1020)$	0.008 ± 0.001	0.005 ± 0.001	1.15

we have used our own π^0, η and ω data, measured at $3.1 \leq y \leq 3.7$, and applied an improved parameterization [11] that allows to fit in particular the regions of very low $p_\perp$ which dominate the integrated production cross sections. For the ρ we use the distribution of the ω. The ϕ and η' $p_\perp$ spectra are generated by scaling the $p_\perp$ distribution of the η with transverse mass. It is important to note that for our experiment any model of $p_\perp$ distributions in reasonable agreement with data will lead to similar dilepton mass distributions. Main reason is the very low $p_\perp$-cut (50 MeV/c) on tracks which does not cut into the parent $p_\perp$ distribution, except for the π°. An uncertainty of the dilepton spectrum is therefore introduced only because the spectrometer acceptance varies with the dilepton $p_\perp$, the error is less than 8% and depends on the dilepton mass.

The results of our generator have been scaled to p–nucleus reactions under the assumption that the relative particle abundances remain unchanged. This assumption is corroborated by our own data [11] for π^0, η and ω. In addition, the $p_\perp$ distributions are modified according to $\sigma_{pA} = A^{\alpha(p_\perp)} \cdot \sigma_{pp}$. Based on the similarity of $\alpha(p_\perp)$ for π^0 and η found in our experiment [11] we use a universal function $\alpha(p_\perp)$ for all mesons. The maxima of the rapidity distributions for all mesons are shifted towards target rapidity by a fixed Δy of 0.3 and 1 for p–Be and p–Au, respectively, keeping the kinematic limits fixed. The values of Δy have been deduced from the summary report by Busza and Ledoux [21]. For p–Be the uncertainty of the rapidity shift gives a negligible effect on the particle abundances in our acceptance compared to the error of the production cross sections. In the case of p–Au the situation is different. While for pions the shift is rather well established, for higher mass particles a smaller shift can not be excluded. We have quantified the uncertainty by shifting all particles except π° only half a unit towards target rapidity. The ω/π° ratio is reduced by about 15% and the dilepton yield will drop accordingly. For lighter mesons the effect is smaller since the rapidity distribution is less narrow.

All decays considered in our generator are listed in Table 5. The branching ratios are taken from the 1996 review of particle properties [22]. For the Dalitz decays, we use the Kroll–Wada expression [23] multiplied by the form factor fitted to the data measured by the LEPTON-G collaboration [18] (see also the review article [19]). The

Table 5. Meson decays with e^+e^- in the final state considered in our generator. Shown are the branching ratios and the slope of the π^0 and η form factor $b = (dF/dq^2)|_{q^2\approx 0}$ and the two parameters of a Breit–Wigner function $|F(q^2)|^2 = a^4/((a^2 - q^2)^2 + a^2b^2)$ fitted to the Lepton-G data in case of the heavier mesons

Decay	**Branching ratio**	**Form factor**
$\pi^0 \to e^+e^-\gamma$	$(1.198 \pm 0.032)\%$	pole approximation $b = 5.5$ GeV^{-2}
$\eta \to e^+e^-\gamma$	$(5.0 \pm 1.2) \cdot 10^{-3}$	pole approximation $b = (1.9 \pm 0.4)$ GeV^{-2}
$\rho \to e^+e^-$	$(4.44 \pm 0.21) \cdot 10^{-5}$	
$\omega \to e^+e^-$ $\omega \to \pi^0e^+e^-$	$(7.15 \pm 0.19) \cdot 10^{-4}$ $(5.9 \pm 1.9) \cdot 10^{-4}$	Breit–Wigner $a = (0.65 \pm 0.02)$ GeV $b = 0.05$ GeV
$\phi \to e^+e^-$ $\phi \to \eta e^+e^-$	$(3.09 \pm 0.07) \cdot 10^{-4}$ $(1.3^{+0.8}_{-0.6}) \cdot 10^{-4}$	
$\eta' \to e^+e^-\gamma$	$\sim 5.6 \cdot 10^{-4}$	Breit–Wigner $a = 0.76$ GeV $b = 0.10$ GeV

form factors of the π^0 and η Dalitz decays are expressed in terms of the slope parameter $b = (dF/dq^2)|_{q^2\approx 0}$ of the so-called pole approximation, i.e. $F(q^2) = (1 - q^2b)^{-1}$. The form factors of the ω and η' Dalitz decays are fitted with a Breit–Wigner function $|F(q^2)|^2 = a^4/((a^2 - q^2)^2 + a^2b^2)$ in order to describe the resonant behavior in a proper way. The parameters used and their errors are listed in Table 5. The latter reflect the uncertainties of the fits due to the limited statistics of the data. The vector meson decays into e^+e^- were generated using the equations of Gounaris and Sakurai [24]. All decays where assumed isotropic except for the Dalitz decays to $e^+e^-\gamma$ which follow a $1 + \cos^2(\theta)$ distribution, where θ is measured with respect to the virtual photon direction.

Associate $c\bar{c}$ production with subsequent semi-leptonic decays of the produced mesons also give rise to genuine lepton pairs. This contribution has been estimated using the PYTHIA Monte-Carlo code [25]. The charm production cross section in the beam energy region around $\sqrt{s} = 20$ GeV is now well established. In addition, kinematic distributions of D-mesons [26] as well as of $D\bar{D}$ pairs [27] are reasonably well produced by PYTHIA using a scaling factor $k = 5$ [28].

Experiments with Be, Al, Cu and W targets show, to high precision, that the charm production cross section scales linearly with the atomic mass number [29]. In order to extrapolate to p–nucleus we therefore scale the p–p calculation by the atomic mass number of the target A: $\sigma_{pA} = A\sigma_{pp}$. The normalization to our data is obtained by scaling with $(\langle dN_{ch}/dy \rangle \sigma_{inel.})^{-1}$ where the inelastic cross section $\sigma_{inel.}$ is taken from [22].

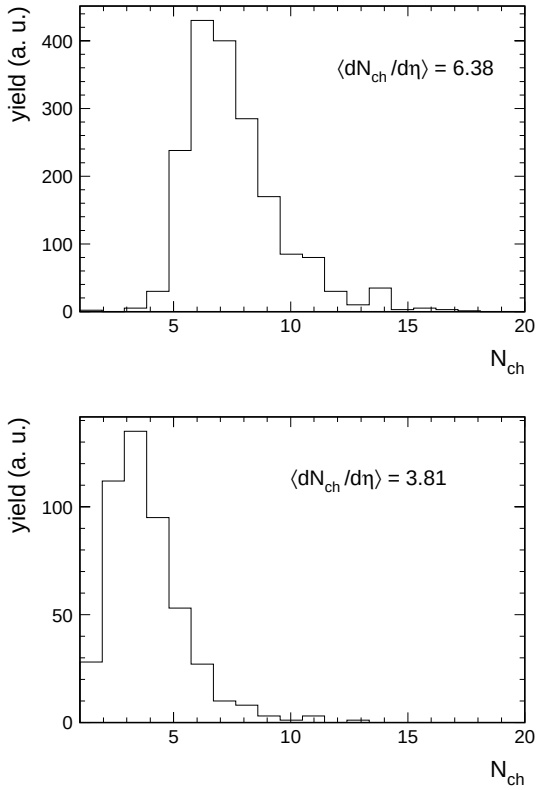

Fig. 13. Charged-particle density distribution of events triggered on electron pairs in p–Be, measured with the SiPD in the pseudo-rapidity interval $2 < \eta < 3$ (top) and the corrected minimum-bias distribution (bottom), see text

In the mass region below 1 GeV/c^2, e^+e^- pairs from associated $D\bar{D}$ decays give a negligible contribution compared to decays of light hadrons (see Fig. 14 and 15). Therefore the uncertainty of the calculation is neglected in the overall error estimate.

7 The measured pair density compared to the expectation from meson decays

7.1 Absolute normalization

In order to compare our data with the e^+e^- pair yield expected from hadron decays, we normalize the data to represent pair density per charged particle density within the rapidity acceptance of $2.1 < \eta < 2.65$,

$$\frac{d^2N_{ee}/d\eta dm}{dN_{ch}/d\eta} = \frac{N_{rec}(m)/N_{events}}{F_T\epsilon_{rec}(m)\langle dN_{ch}/d\eta\rangle \Delta\eta} \quad . \qquad (1)$$

N_{rec} is the number of reconstructed pairs as a function of the invariant pair mass, N_{events} is the total number of analyzed events, ϵ_{rec} is the pair reconstruction efficiency of the off-line analysis, $< dN_{ch}/d\eta >$ is the average number of charged particles per unit of rapidity within the CERES acceptance, $\Delta\eta$ is the CERES fiducial acceptance and F_T is the trigger enrichment factor (see Sect. 2.2).

The $dN_{ch}/d\eta$ distribution for p–Be is shown in the top of Fig. 13. The average is 6.4. This distribution is biased by requiring an e^+e^- pair in the trigger. In order to derive a minimum-bias distribution, two corrections are applied, (a) subtracting the two additional hits caused by the e^+e^- pair and (b) accounting for the fact that the probability to have an electron pair in the event is proportional to the number of charged particles in that event. The minimum bias charged particle distribution obtained after these corrections is shown in the bottom of Fig. 13 for the p–Be data. The average charge multiplicity is then $\langle dN_{ch}/d\eta\rangle = 3.8$ [4]. For p–Au we find $\langle dN_{ch}/d\eta\rangle = 7.0$.

Figures 14 and 15 show the normalized inclusively measured e^+e^- pair spectra in 450 GeV/c p–Be and p–Au collisions together with the various contributions from hadron decays. This 'cocktail' of hadronic contributions is displayed in the figures for the respective colliding systems, both separately, and by their sum. In the figures, the statistical errors are marked by bars, whereas the brackets reflect the systematic uncertainties in the data. The systematic errors on the expected yield from hadron decays are shown as shaded region. Both types of systematic errors are discussed below.

The yield of Fig. 14 falls over 5 orders of magnitude with increasing pair mass. Measured with full pair acceptance, the mass spectrum would be less steep. Given the acceptance $2.1 \leq \eta \leq 2.65$ of the spectrometer, the ratio of e^+e^- pairs to the number of virtual photons is unity only at the lowest masses and drops to 0.1 at masses above a few hundred MeV/c^2. For easy comparison of the p–Be and p–Au data with our A–A collision data, no pair acceptance corrections were done.

7.1.1 Systematic errors of data

Three sources contribute to the systematic uncertainties of the data: (a) the trigger enrichment factor F_T, (b) the off-line pair reconstruction efficiency ϵ_{rec} and (c) the average charged-particle density $\langle dN_{ch}/d\eta\rangle$. The error of the trigger enrichment factor F_T itself depends on the uncertainties of the FLT bias b_{FLT}, the reduction factor R_T and the trigger efficiency ϵ_T. The FLT bias b_{FLT} and the reduction factor R_T are well known from the on-line monitoring. Fluctuations of the measured FLT bias b_{FLT} are shown in Fig. 2. Since the trigger conditions remain unchanged throughout the run these variations point towards some systematic error in the determination of b_{FLT}. One source contributing to changes of b_{FLT} are fluctuations

[4] In our previous publication [7] we have quoted $\langle dN_{ch}/d\eta\rangle = 3.1$ for p–Be which corresponds to the unbiased value in our acceptance, i.e. for an event sample without any restrictions on the charged particle multiplicity. The difference in normalization is less than 5% because the increase in $\langle dN_{ch}/d\eta\rangle$ is counter balanced by a decrease of the first-level trigger bias b_{FLT}. Throughout this paper all numbers refer to actually measured quantities and do no longer involve an extrapolation to unbiased collisions

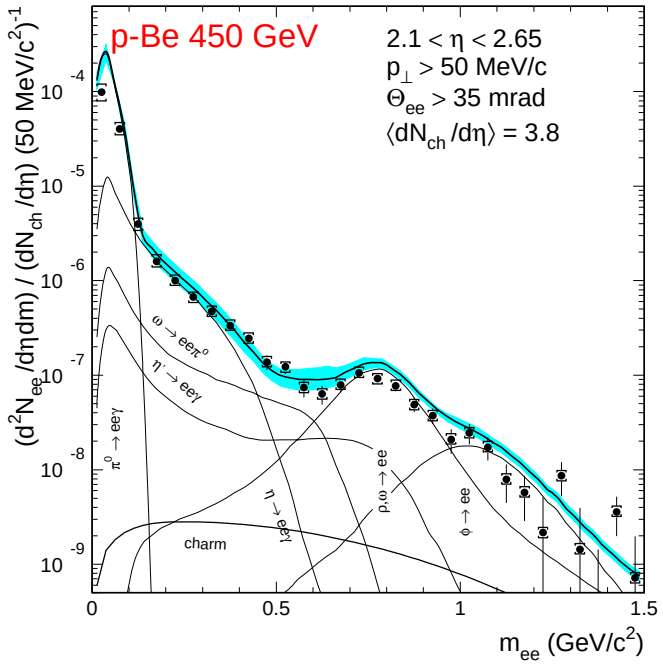

Fig. 14. Invariant e^+e^- mass spectrum in 450 GeV p–Be collisions representing pair density per charged-particle density. Data (*full circles*) with systematic errors in absolute normalization of about 18% (*brackets*), statistical errors (*bars*) negligible below 1 GeV/c^2. The hadronic cocktail of Dalitz- and direct meson decays is shown separately (*thin lines*) and summed up (*thick line*) to the expected hadron decay spectrum. The simulation follows very well the data in view of systematic errors (*shaded area*) that reflect deficiencies in our knowledge on meson production and decay properties. No pair acceptance corrections are applied

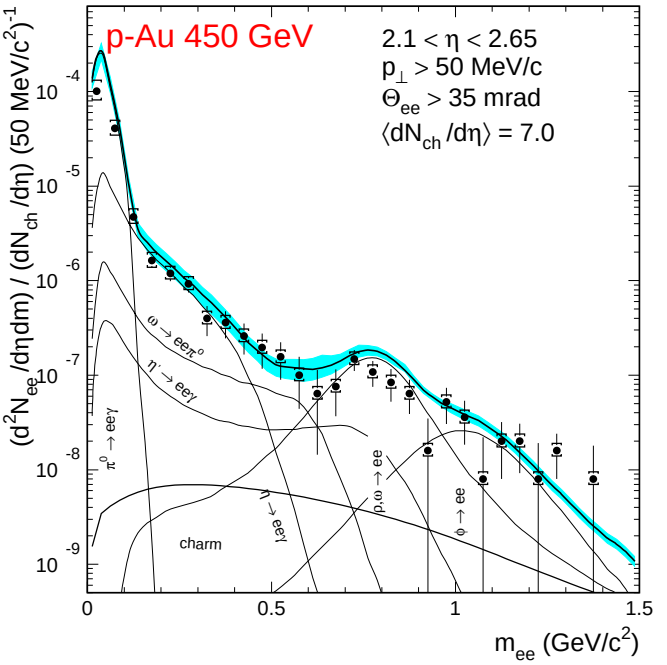

Fig. 15. Invariant e^+e^- mass spectrum in 450 GeV p–Au collisions. Systematic errors are about 21%, statistical errors are no longer negligible. Within these limits, the measured spectrum is well described by neutral meson decays. No pair acceptance corrections are applied. For explanations see Fig. 14

of the $\sim$ 3% non-target interactions with the beam quality, but it can not account for the magnitude of observed variations. We therefore use the RMS spread of the distribution as a measure of the systematic error of b_{FLT}, which is 9%.

The variations of R_T over the data taking period mostly results from gain variations in the UV detectors. The reduction factor R_T, the trigger efficiency ϵ_T and the reconstruction efficiency ϵ_{rec} are strongly correlated. The uncertainty in the product of the trigger enrichment factor F_T and the pair reconstruction efficiency ϵ_{rec} from the gain variations amount to 6%. This error is obtained from the variation of $R_T \cdot \epsilon_T \cdot \epsilon_{rec}$ for a $\pm\sigma$ change of the average UV-detector gain, which is about 13%.

Uncertainties in the description of the detector response in the Monte-Carlo simulation result in an error of the absolute values ϵ_T and ϵ_{rec}, even at fixed gain. The error of $\epsilon_T \cdot \epsilon_{rec}$ has been investigated by comparing results from independently optimized Monte-Carlo simulations. In addition, the correctness of the Monte-Carlo simulation was checked by investigating the sensitivity of the final result to small variations of the background rejection cuts. The uncertainty of the product $\epsilon_T \cdot \epsilon_{rec}$ is estimated to be $\sim$ 8%.

The error of the average charged-particle density $\langle dN_{ch}/d\eta \rangle$ measurement results from the uncertainty of (a) the contribution of the electron and positron hits, (b) pile-up losses due to the finite pad size, (c) the empty target correction, and (d) the acceptance correction. Altogether, we estimate the systematic uncertainty of $\langle dN_{ch}/d\eta \rangle$ to $\sim$ 10% and $\sim$ 15% in p–Be and p–Au, respectively. The combined systematic uncertainty of the absolute normalization is about 17% in p–Be and 20% in p–Au.

7.1.2 Systematic errors of the generator

The uncertainties in the generator concerning production of neutral mesons and their decay into electron pairs are shown as the shaded band in Figs. 14 and 15. They arise from (a) the relative production cross section shown in Table 4, (b) the branching ratios and/or electromagnetic form factors given in Table 5, (c) the uncertainty of the π^0/N_{ch} ratio which is less than 5% [20], and (d) the error related to the parameterization of the $p_\perp$ and y distributions estimated to be 8% for p–Be and 17% for p–Au. The errors of (a), (b), and (d) lead to a mass-dependent uncertainty that for p–Be amounts to about 23% below 450 MeV/c^2 and is dominated by the poorly known branching $\eta \to e^+e^-\gamma$. At the upper end, $m > 750$ MeV/c^2, the systematic error is reduced to 14% reflecting the comparatively well-known relative production cross sections of the ρ and ω, and their branching ratios into e^+e^- pairs.

The intermediate mass range is populated strongly by the ω Dalitz decay $\omega \to e^+e^-\pi^0$, and it is the rather large uncertainty in the electromagnetic transition form factor involved that causes the width of the error band to reach 40% here. For p–Au the systematic errors are somewhat larger.

Within these errors, the measured mass spectra for p–Be and p–Au with absolute normalization to charged particles are in very good agreement with the spectra expected from neutral-meson decays. In the ρ/ω mass region both spectra might indicate a small suppression in yield compared to the generator which might point to a destructive ρ/ω interference. This interference was directly observed in resonant $e^+e^- \to \pi^+\pi^-$ scattering at Novosibirsk [30]. In the hadro production of lepton pairs the situation is much less clear, although HELIOS-1 reports indeed some preference for a destructive interference from the high-statistics muon data [5]. We have not included the ρ/ω interference in our generator.

The π° Dalitz decay does not contribute to masses above 200 MeV/c^2, and we have normalized it independently from the η. In the mass region below 200 MeV/c^2, the pair spectrum is overwhelmingly π^0 Dalitz decay. In view of the problems in triggering on, and in reconstructing pairs that soft, the excellent agreement between simulation and data evident from Fig. 16 might be fortuitous. The generator was normalized by the number of completely measured and reconstructed π^0 Dalitz decays. However, the relative normalization does not comply with the accepted π^0/η ratio of Table 4. The explanation is probably given by the fact that the major part of the electron pairs from π^0 Dalitz are suppressed by the trigger and the $p_\perp$ cut.

7.2 Normalization relative to the exclusively measured η Dalitz decay

A certain fraction of the electron pairs from p–Be which we have reconstructed was in fact registered as $e^+e^-\gamma$ or $e^+e^-\pi^\circ$ Dalitz decays: the respective photons were detected in the BaF_2 calorimeter coincident with the pair, and all four-momenta met the kinematic requirements imposed by the decaying mesons. Clearly, given the number of exclusively reconstructed mesons, it is straight-forward to predict the number of pairs that should be observed in the simultaneous inclusive e^+e^- measurement, provided we know the acceptance and photon reconstruction efficiency of the calorimeter. Since all conditions of beam, trigger, and pair reconstruction are identical in the exclusive and inclusive data sets and therefore cancel, this relative normalization is potentially more accurate than the previously described absolute method.

In the invariant mass range $0.2 < m < 0.5$ GeV/c^2 the η Dalitz decay strongly dominates the mass spectrum. We were able to reconstruct η mesons from the exclusive data with sufficient statistical accuracy, unlike the ω mesons. Therefore, we have based our relative normalization on the η Dalitz decay.

The inclusive p–Be data are plotted together with the mass spectra generated for the various neutral-meson decays in Fig. 16. The absolute scale of the generator cocktail was set to reproduce the measured number of the reconstructed η Dalitz decays (Table 2). The contributions of all heavier mesons are scaled to the η Dalitz decay according to the production cross sections listed in Table 4.

The derived spectrum of electron pairs from hadron decays is in excellent agreement with the measured inclusive e^+e^- pair spectrum. In magnitude, the ratio of integral yields for $m > 200$ MeV/c^2 of data to that of the generator is 1.04.

Again, the statistical errors of the inclusive data are marked by bars. In contrast to the same data displayed in Fig. 14, systematic errors of data points are omitted here, since the major contribution to systematic errors, trigger efficiency and pair reconstruction efficiency, do not enter the comparison between inclusive and exclusive data. However, those systematic errors do affect the absolute scale of the ordinate in Fig. 16, which therefore is uncertain within ±17%.

The shaded region indicates the systematic error on the total contribution from hadron decays and the systematic uncertainties on the absolute normalization of the generator. Those uncertainties arise from (a) the photon reconstruction efficiency, (b) the acceptance correction, (c) the mass dependence of the pair reconstruction efficiency, and (d) the measurement of the Dalitz decay signal. There are three important contributions to the error in the mass region below 450 MeV/c^2, the statistical (9.7%) error of the exclusive η-Dalitz decay reconstruction, the systematic error (12.6%) originating from the background subtraction (see Sect. 5.2), and the parameterization error (8%). Including all other smaller contributions we estimate a total error of $\sim$ 18%.

Compared to the absolute normalization discussed in Sect. 7.1, the relative normalization introduces larger errors above 0.8 GeV/c^2. The yield of the relevant particles (ρ, ω, η' and ϕ) is tied to the η yield so that the $\eta \to e^+e^-\gamma$ branching ratio enters with its considerable uncertainty. The overall error at masses above 0.8 GeV/c^2 is about $\sim$ 30%. The absolute normalization is advantageous here, yielding a total error of only $\sim$ 22%, composed of 14% generator-induced and 17% data-induced systematic errors.

8 Results and conclusions

The mass spectrum of e^+e^- pairs from p–Be collisions can be reproduced by Dalitz and direct decays of the neutral mesons produced. We arrive at this conclusion on two largely independent ways:

(i) The measured pair density per charged-particle density for $m > 200$ MeV/c^2 is compared to a generator simulation of production and decay of the relevant neutral mesons as well as their detection and reconstruction, without any freedom in absolute scale. The comparison rests upon the independently evaluated pair acceptance, trigger enrichment and ring reconstruction efficiencies; on

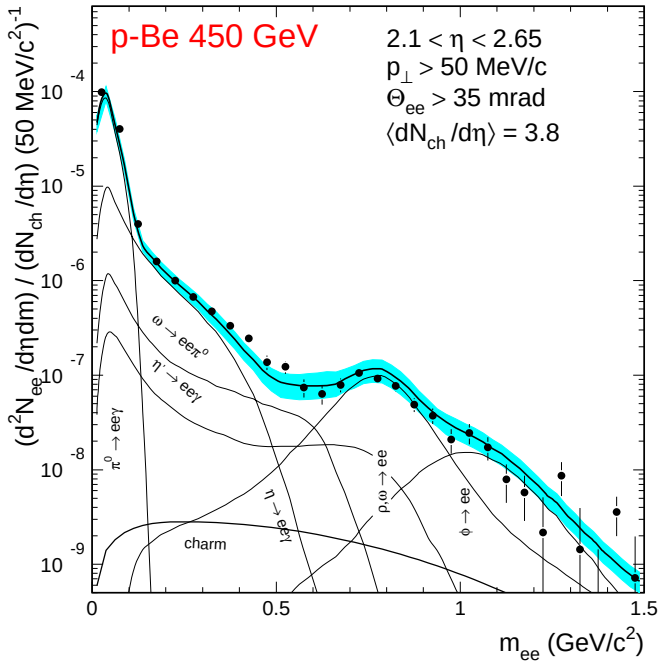

Fig. 16. Invariant e^+e^- mass spectrum in 450 GeV p–Be collisions showing the data (*full circles*) and the various contributions from hadron decays. The absolute scale of the generator cocktail was set to reproduce the exclusively measured π^0 and η Dalitz decays independently (see text). The *shaded region* indicates the systematic error on the summed contributions and contains also the uncertainties (statistical and systematic) of the exclusive η measurement. The error on the absolute scale is ±17%. No pair acceptance corrections are applied

the relevant cross section ratios of neutral mesons with respect to π^0 (Table 4) which were to a large extent determined by the photon-exclusive measurement within the same experiment down to very low $p_\perp$; and on the ratio number of π^0's per charged particle. It is quite remarkable that data and simulation agree so well in shape and on absolute scale. We like to see this as an expression of the validity of our present understanding of the CERES spectrometer, the trigger action, and the off-line event reconstruction.

The data points are systematically uncertain in absolute normalization to within 17%. To the hadron decay simulation has been attached a band of systematic errors that is 23% below 450 MeV/c^2, 14% above 750 MeV/c^2, and grows to 40% in a narrow region from 500MeV/c^2 to 700 MeV/c^2 where the poorly known ω-Dalitz form factor dominates.

(ii) By comparing the number of η mesons reconstructed from $e^+e^-\gamma$ events to the number of inclusively measured electron pairs in the η-Dalitz region, all instrumental uncertainties related to the e^+e^- measurement cancel (trigger enhancement, pair reconstruction efficiency, etc.). What remains of systematic uncertainties relates to the photon reconstruction efficiency and background subtraction. By use of the generator, the contributions of other mesons are scaled to that of the η using the above-mentioned cross section ratios.

The spectrum simulated for hadron decays agrees very well with our p–Be data. There are no more systematic data errors since we have absorbed all uncertainties of the exclusive Dalitz decay reconstruction into the generator band. Below 450 MeV/c^2 the agreement is close to perfect, expressed by an error band of the generator of 18%. This is quite a significant improvement over the total uncertainty of about 29% in the absolute method (i), which is compounded of 23% in the generator and 17% systematic error in the data. Unfortunately, the improved accuracy of the relative-normalization method holds only over the mass range dominated by the η-Dalitz decay, i.e. below 450 MeV/c^2.

Adopting the most advantageous normalization in the respective mass ranges for p–Be, we conclude as follows: the measured pair spectrum below 450 MeV/c^2 agrees to within 18% systematic errors with the expectation from neutral-meson decays; above 750 MeV/c^2 such agreement can be stated within a combined systematic uncertainty of data (17%) and simulation (14%) of 22%. In between, where the ω-Dalitz contribution is dominant, the uncertainty in the transition form factor, increases the error band to about ±40%.

We like to state the result in terms of the largest percentage fractions of unconventional sources that are consistent with our data analysis. In the mass range between 200 MeV/c^2 and 450 MeV/c^2 the limit is 23%, in the mass range above 750 MeV/c^2 it is 28%, both at 90% confidence level. With the exception of the ω-Dalitz mass range, the present experiment has significantly reduced the error margins compared to the e^+e^- results of HELIOS-1, although not to the extent we had been planning for.

Despite considerably larger errors, both systematic – as no $e^+e^-\gamma$ data have been taken – and statistical due to the much smaller data sample, it can be stated that the p–Au invariant mass spectrum of electron pairs is also well described by neutral meson decays. This new finding of no enhancement in p–A collisions over the hadronic contributions, on a 40% level, is especially interesting in view of the strong enhancement observed for low-mass electron pairs [7] and muon pairs [31] in S–induced collisions, and more recently, of comparable magnitude in central Pb–Au collisions [32].

Acknowledgements. We would like to express our sincere gratitude to the specialists of the CERN SPS. We are grateful for support by Deutsches Bundesministerium für Bildung, Wissenschaft, Forschung und Technologie (BMBF) under the contracts No. 06 HD 525 I and No. 06 GI 475 I (3), by Gesellschaft für Schwerionenforschung (GSI), by the German-Israeli Foundation for Scientific Research and Development under contract I-366-194, by the Israel Science Foundation, by the U.S. Department of Energy under Contract No. DE-AC02-76CH00016, and by a research grant from the Clarisse and Cornelius Gustav Memorial Fund.

References

1. V. V. Abramov et al., Phys. Lett. B**64** (1976) 365; K.J. Anderson et al., Phys. Rev. Lett. **37** (1976) 799; M.R. Adams et al., Phys. Rev. D **27** (1983) 1977; P.A. Baker, Phys. Rev. Lett. **41** (1978) 1207; D. Blockus, Nucl. Phys. B**201** (1982) 205; T. Åkesson et al., Phys. Lett. B**192** (1987) 463
2. R.N. Cahn, Phys. Rev. D **7** (1973) 247; R. Rückl, Phys. Lett. B **64** (1976) 39
3. J.D. Bjørken und H. Weisberg, Phys. Rev. D **13** (1976) 1405; V. Černý et al., Acta Phys. Pol. B**9** (1978) 901; V. Černý et al., Phys. Rev. D **24** (1981) 652
4. E.V. Shuryak, Phys. Lett. B**78** (1978) 150
5. T. Åkesson et al., Z. Phys. C **68** (1995) 47; R.J. Veenhof, Ph.D. Thesis, University of Amsterdam (1993)
6. R. Baur, Doctoral Thesis, University of Heidelberg (1994)
7. G. Agakichiev et al., Phys. Rev. Lett. **75** (1995) 7; G. Agakichiev et al., Nucl. Phys. A**590** (1995) 103c
8. CERN SPSLC 92-48, Addendum II to Proposal SPSC/P237 (1992)
9. Ch. Fuchs, Doctoral Thesis, University of Heidelberg (1996)
10. G. Tel–Zur, Ph.D. Thesis, Weizmann Institute of Science, Rehovot (1996)
11. G. Agakichiev et al., this issue of Eur. Phys. J. C
12. R. Baur et al., Nucl. Instr. and Meth. A **343** (1994) 87
13. R. Novotny, IEEE Trans. Nucl. Sci. **38** (1991) 379
14. T.F. Günzel et al., Nucl. Instr. Meth. A **316** (1992) 259
15. J. Gläß et al., IEEE Trans. Nucl. Sci. **37** (1990) 241
16. P. Holl et al., CERN/SPSLC 94-1 Proposal SPSLC P280 (1994)
17. D. Drijard et al., Nucl. Instr. and Meth. **225**c (1984) 367
18. R.I. Dzhelyadin et al., Phys. Lett. **102**B (1980) 548
19. L.G. Landsberg, Phys. Rep. **128** (1985) 301
20. M. Aguilar–Benitez et al., Z. Phys. C **50** (1991) 405
21. W. Busza and R. Ledoux, Ann. Rev. Nucl. Part. Sci. **38** (1988) 119
22. R. M. Barnett et al.,Phys. Rev. D**54** (1996) 1
23. N. Kroll and W. Wada, Phys. Rev. **98** (1955) 1355
24. G.J. Gounaris and J.J. Sakurai, Phys. Rev. Lett. **21** (1968) 244
25. T. Sjostrand, Comp. Phy. Comm. **82** (1994) 74
26. G. A. Alves et al., Phys. Rev. Lett. **77** (1996) 2392
27. M. Adamovich et al., preprint CERN–PPE/96–180
28. P. Braun-Munzinger et al., nucl-ex/97040111, submitted to Eur. Phys. J. C
29. G. A. Alves et al., Phys. Rev. Lett. **70** (1993) 722; M. J. Leitch et al., Phys. Rev. Lett. **72** (1994) 2542
30. L.M. Barkov, Nucl. Phys. B**256** (1985) 365
31. M. Masera (Helios-3 Collaboration), Nucl. Phys. A**590** (1995) 93c
32. G. Agakichiev et al., Nucl. Phys. A**610** (1996) 317c